tubulin, 4.5 μM N-ethylmaleimide (NEM)-tubulin[26], 1 mM GTP and 2 mM dithiothreitol, followed by incubation at 35 °C for 20 min. NEM-tubulin was added to inhibit minus-end growth, resulting in rhodamine-microtubule growth from the plus-end of the Cy5-labelled seeds only. Polymerized microtubules were stabilized using 10 μM paclitaxel (Sigma).

In vitro assays

Assays were performed at 21 °C using an epi-illuminated wide-field fluorescence microscope capable of optical trapping and laser-darkfield detection as described elsewhere[27]. Excitation light (532 nm) was coupled into the objective with a polychromatic dichroic mirror (532/633PC, Chroma), allowing combined excitation with a 633-nm HeNe laser (Coherent) as well as transmission darkfield imaging with a 650-nm diode laser (Roithner Lasertechnik). Emission was first short-pass filtered (Chroma E750sp), further filtered with holographic notch filters against 532-nm and 633-nm light (Kaiser Optical Systems HNPF-532 and HNPF-632.8), separated with a dichroic mirror (645DCXRlp, Chroma) and imaged side-by-side on the CCD-camera, allowing simultaneous imaging of rhodamine emission and either darkfield light or Cy5 emission. For darkfield detection of axonemes, we used a darkfield condensor (Nikon) in combination with a decreased numerical aperture (NA) of the objective to block illumination light. Trapping experiments required full NA and hence we used fluorescence imaging of axonemes in those experiments. The trapping laser was used at 850-nm at a power of typically 150 mW in the sample.

Hydrophobic sample chambers were assembled by joining dimethyl-dichlorosilane-treated slides and coverslips using two layers of double-stick tape (~150-μm inner height). A chamber was first incubated with axonemes in PEM80 (80 mM PIPES, 1 mM EGTA, 2 mM $MgCl_2$, pH 6.8) for 10 min, then blocked by washing with 5 volumes of PEM80 with amphiphilic copolymers (0.2% (w/v) Pluronic F108, BASF) and 0.1% (w/v) polyethylene-*block*-poly(ethylene glycol) (PEPEG, Aldrich). Finally, the chamber was filled with the motility sample, consisting of PEM80 with microtubules, 6–12 μg ml^{-1} Eg5, 6–10 mM ATP, 4 mM dithiothreitol, 25 mM glucose, 20 μg ml^{-1} glucose oxidase, 35 μg ml^{-1} catalase, 10 μM paclitaxel, 0.2% (w/v) Pluronic F108, and in some cases 0.1% (w/v) PEPEG and/or 0.1% (w/v) methyl cellulose (Fluka). For trapping experiments, 1-μm fluorescent silica beads (Kisker Biotech) treated with anti-α-tubulin antibodies (Sigma) were added, and methyl cellulose was left out. Measurements at high salt were performed with 150 mM sodium acetate in PEM80 or 150 mM potassium acetate in PEM12 (equivalent to PEM80, except with 12 mM PIPES), together with a two- to threefold increase in Eg5 concentration. This was necessary to compensate for a lower probability of microtubule capture at higher salt. For controls without axonemes, sample mix was used with an increased concentration of both microtubules and Eg5 (full-length or truncated) to enhance crosslinking in solution.

Assays with polarity-marked microtubules were performed in sample chambers of 5-μm inner height (set by the addition of spacer beads, Seradyn) to confine microtubules near the focal plane. Both surfaces were pre-incubated with the copolymers and dried, after which the sample mix was put onto one surface and covered with the other. Surface blocking was not perfect in these samples, but good enough to keep sufficient microtubules and motors in solution. Imperfect blocking was an advantage because, for stable imaging, we could choose events in which at least one microtubule was partially stuck to the surface.

Surface gliding assays were performed under the same buffer conditions but without surface blocking.

Image analysis

Digital images were analysed using custom-written routines in LabVIEW (National Instruments). Speeds were determined by measuring displacement relative to a reference point on one of the filaments. For Fig. 3, every 5–10 frames were averaged to reduce the number of frames. Microtubules were automatically tracked and the position of the trailing end was measured relative to its final position.

Received 13 January; accepted 2 March 2005; doi:10.1038/nature03503.

1. Scholey, J. M., Brust-Mascher, I. & Mogilner, A. Cell division. *Nature* **422,** 746–752 (2003).
2. Compton, D. A. Spindle assembly in animal cells. *Annu. Rev. Biochem.* **69,** 95–114 (2000).
3. Kashina, A. S., Rogers, G. C. & Scholey, J. M. The bimC family of kinesins: essential bipolar mitotic motors driving centrosome separation. *Biochim. Biophys. Acta* **1357,** 257–271 (1997).
4. McIntosh, J. R., Hepler, P. K. & Vanwie, D. G. Model for mitosis. *Nature* **224,** 659–663 (1969).
5. Sharp, D. J., Rogers, G. C. & Scholey, J. M. Microtubule motors in mitosis. *Nature* **407,** 41–47 (2000).
6. Brust-Mascher, I. & Scholey, J. M. Microtubule flux and sliding in mitotic spindles of *Drosophila* embryos. *Mol. Biol. Cell* **13,** 3967–3975 (2002).
7. Kashina, A. S. *et al.* A bipolar kinesin. *Nature* **379,** 270–272 (1996).
8. Sharp, D. J. *et al.* The bipolar kinesin, KLP61F, cross-links microtubules within interpolar microtubule bundles of *Drosophila* embryonic mitotic spindles. *J. Cell Biol.* **144,** 125–138 (1999).
9. Sawin, K. E., Leguellec, K., Philippe, M. & Mitchison, T. J. Mitotic spindle organization by a plus-end-directed microtubule motor. *Nature* **359,** 540–543 (1992).
10. Wilde, A. *et al.* Ran stimulates spindle assembly by altering microtubule dynamics and the balance of motor activities. *Nature Cell Biol.* **3,** 221–227 (2001).
11. Mayer, T. U. *et al.* Small molecule inhibitor of mitotic spindle bipolarity identified in a phenotype-based screen. *Science* **286,** 971–974 (1999).
12. Miyamoto, D. T., Perlman, Z. E., Burbank, K. S., Groen, A. C. & Mitchison, T. J. The kinesin Eg5 drives poleward microtubule flux in *Xenopus laevis* egg extract spindles. *J. Cell Biol.* **167,** 813–818 (2004).
13. Kwok, B. H., Yang, J. G. & Kapoor, T. M. The rate of bipolar spindle assembly depends on the microtubule-gliding velocity of the mitotic kinesin Eg5. *Curr. Biol.* **14,** 1783–1788 (2004).
14. Kapoor, T. M. & Mitchison, T. J. Eg5 is static in bipolar spindles relative to tubulin: evidence for a static spindle matrix. *J. Cell Biol.* **154,** 1125–1133 (2001).
15. Kapoor, T. M. & Mitchison, T. J. Allele-specific activators and inhibitors for kinesin. *Proc. Natl Acad. Sci. USA* **96,** 9106–9111 (1999).
16. Howard, J., Hudspeth, A. J. & Vale, R. D. Movement of microtubules by single kinesin molecules. *Nature* **342,** 154–158 (1989).
17. Desai, A., Verma, S., Mitchison, T. J. & Walczak, C. E. Kin I kinesins are microtubule-destabilizing enzymes. *Cell* **96,** 69–78 (1999).
18. Crevel, I. M., Alonso, M. C. & Cross, R. A. Monastrol stabilises an attached low-friction mode of Eg5. *Curr. Biol.* **14,** R411–R412 (2004).
19. Stock, M. F., Chu, J. & Hackney, D. D. The kinesin family member BimC contains a second microtubule binding region attached to the N terminus of the motor domain. *J. Biol. Chem.* **278,** 52315–52322 (2003).
20. Crevel, I., Lockhart, A. & Cross, R. A. Kinetic evidence for low chemical processivity in ncd and Eg5. *J. Mol. Biol.* **273,** 160–170 (1997).
21. McDonald, H. B., Stewart, R. J. & Goldstein, L. S. B. The kinesin-like ncd protein of *Drosophila* is a minus end-directed microtubule motor. *Cell* **63,** 1159–1165 (1990).
22. Chui, K. K. *et al.* Roles of two homotetrameric kinesins in sea urchin embryonic cell division. *J. Biol. Chem.* **275,** 38005–38011 (2000).
23. Nislow, C., Lombillo, V. A., Kuriyama, R. & McIntosh, J. R. A plus-end-directed motor enzyme that moves antiparallel microtubules *in vitro* localizes to the interzone of mitotic spindles. *Nature* **359,** 543–547 (1992).
24. Gibbons, I. R. & Fronk, E. Latent adenosine-triphosphatase form of dynein-1 from sea urchin sperm flagella. *J. Biol. Chem.* **254,** 187–196 (1979).
25. Williams, R. C. & Lee, J. C. Preparation of tubulin from brain. *Methods Enzymol.* **85,** 376–385 (1982).
26. Hyman, A. A. Preparation of marked microtubules for the assay of the polarity of microtubule-based motors by fluorescence. *J. Cell Sci.* **14** (suppl.), 125–127 (1991).
27. van Dijk, M. A., Kapitein, L. C., van Mameren, J., Schmidt, C. F. & Peterman, E. J. G. Combining optical trapping and single-molecule fluorescence spectroscopy: Enhanced photobleaching of fluorophores. *J. Phys. Chem. B* **108,** 6479–6484 (2004).

Supplementary Information accompanies the paper on **www.nature.com/nature**.

Acknowledgements We thank I. Schaap for purifying tubulin, S. Calmat and J. Hendriks for assistance with FPLC chromatography, J. van Mameren for help with software, and M. Korneev, M. Mazur and K. Zabrocka for help with surface chemistry and motility controls. L.C.K. and E.J.G.P. are supported by a VIDI fellowship to E.J.G.P. from the Research Council for Earth and Life Sciences (ALW), with financial aid from the Netherlands Organization for Scientific Research (NWO). T.M.K., B.H.K., J.H.K. are grateful to the NIH/NIGMS for support. Additional support was provided by the Foundation for Fundamental Research on Matter (C.F.S.) and a Research Grant from the Human Frontier Science Program (C.F.S. and T.M.K.).

Competing interests statement The authors declare that they have no competing financial interests.

Correspondence and requests for materials should be addressed to E.J.G.P. (erwinp@nat.vu.nl) or T.M.K. (kapoor@mail.rockefeller.edu).

A synthetic gene–metabolic oscillator

Eileen Fung[1,2], Wilson W. Wong[1], Jason K. Suen[1], Thomas Bulter[1], Sun-gu Lee[1] & James C. Liao[1,2]

[1]*Department of Chemical Engineering and* [2]*Biomedical Engineering Interdepartmental Program, University of California–Los Angeles, Los Angeles, California 90095, USA*

Autonomous oscillations found in gene expression and metabolic, cardiac and neuronal systems[1–4] have attracted significant attention both because of their obvious biological roles and their intriguing dynamics. In addition, *de novo* designed[5–12] oscillators[13,14] have been demonstrated, using components that are not part of the natural oscillators. Such oscillators are useful in testing the design principles and in exploring potential applications not limited by natural cellular behaviour[15]. To achieve transcriptional and metabolic integration characteristic of natural oscillators, here we designed and constructed a synthetic circuit in *Escherichia coli* K12, using glycolytic flux to generate oscillation through the signalling metabolite acetyl phosphate. If two metabolite pools are interconverted by two enzymes that are placed under the transcriptional control of acetyl phosphate, the system oscillates when the glycolytic rate exceeds a critical value. We used bifurcation analysis to identify the boundaries of

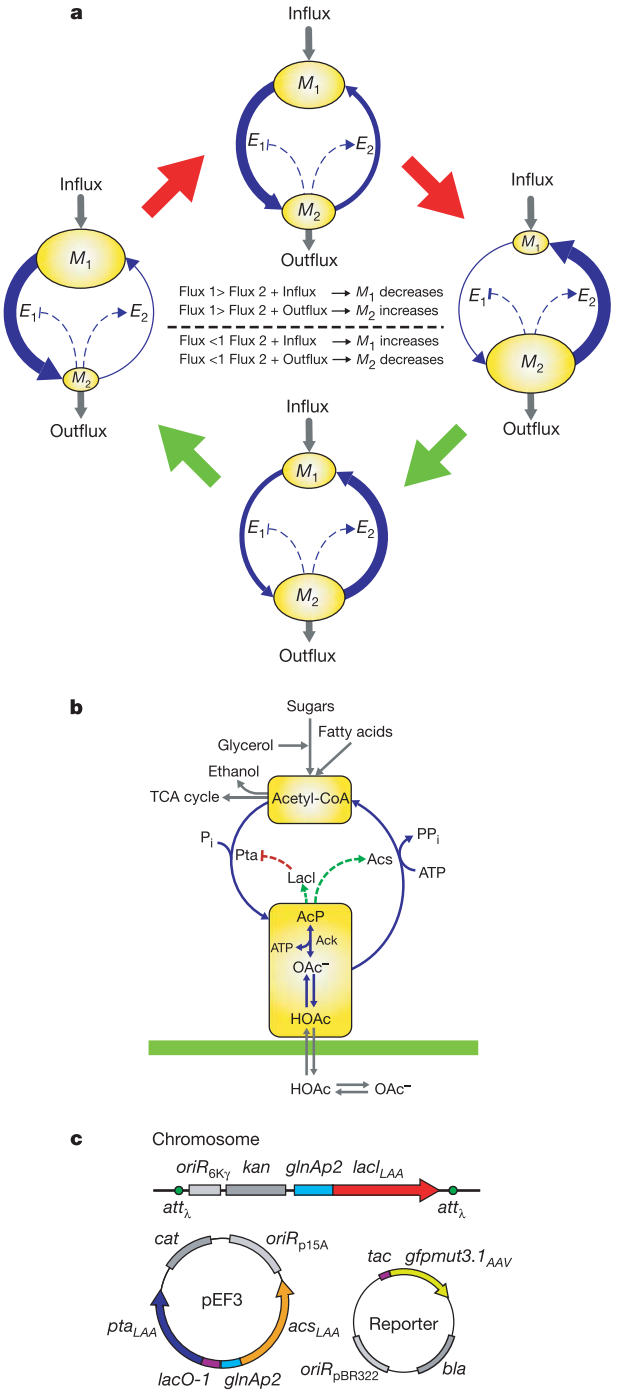

Figure 1 The design and construction of the metabolator. **a**, Conceptual diagram of the oscillatory dynamics, highlighting the two metabolite pools (M_1 and M_2) and their controls. Solid lines indicate metabolic fluxes. Dashed lines indicate positive (arrow) and negative (blunt bar) transcriptional or translational regulation. Input metabolic flux increases M_1. E_1 drives M_1 to M_2. Accumulation of M_2 represses E_1 and upregulates E_2 expression. Low E_1 and high E_2 levels drive M_2 to M_1 and a new cycle begins. **b**, Biological realization of the conceptual design in **a**. The yellow boxes highlight the two metabolic pools, M_1 and M_2. Ack, acetate kinase; AcP, acetyl phosphate; Acs, acetyl-CoA synthetase; OAc^-, acetate; Pta, phosphate acetyltransferase. **c**, *E. coli* strain and plasmid constructs. The *lacI* gene under the control of the *glnAp2* promoter was inserted into the *E. coli* chromosome at the lambda attachment site (att_λ) (see Methods). A degradation tag was fused to the 3′-end of the gene to reduce the stability of LacI ($lacI_{LAA}$). The pEF3 plasmid expresses low-stability Pta (pta_{LAA}) and Acs (acs_{LAA}), which are controlled by the *lacO-1* and *glnAp2* promoters, respectively. The reporter plasmid expresses an intermediate-stability GFP variant ($gfpmut3.1_{AAV}$) under the control of the *tac* promoter. *kan*, *cat* and *bla* are genes for resistance to kanamycin, chloramphenicol and ampicillin, respectively.

oscillation, and verified these experimentally. This work demonstrates the possibility of using metabolic flux as a control factor in system-wide oscillation, as well as the predictability of a *de novo* gene–metabolic circuit designed using nonlinear dynamic analysis.

Our design of this oscillatory circuit, termed the metabolator, integrates transcriptional regulation with metabolism. This is in contrast with the yeast glycolytic oscillator[1,4], which does not involve transcriptional regulation, as well as previous synthetic gene expression oscillators, which were independent of metabolism[13,14]. The conceptual design of the metabolator consists of a flux-carrying network with two interconverting metabolite pools (M_1 and M_2) catalysed by two enzymes (E_1 and E_2), the expressions of which are negatively and positively regulated by M_2, respectively (Fig. 1a). In the first stage, when the level of M_2 is low, E_1 is expressed and E_2 is not. A high input metabolic flux rapidly drives M_1 to M_2. Accumulation of M_2 represses E_1 and upregulates E_2. When the backward reaction rate exceeds the sum of the forward reaction rate and the output rate, the level of M_2 decreases and the

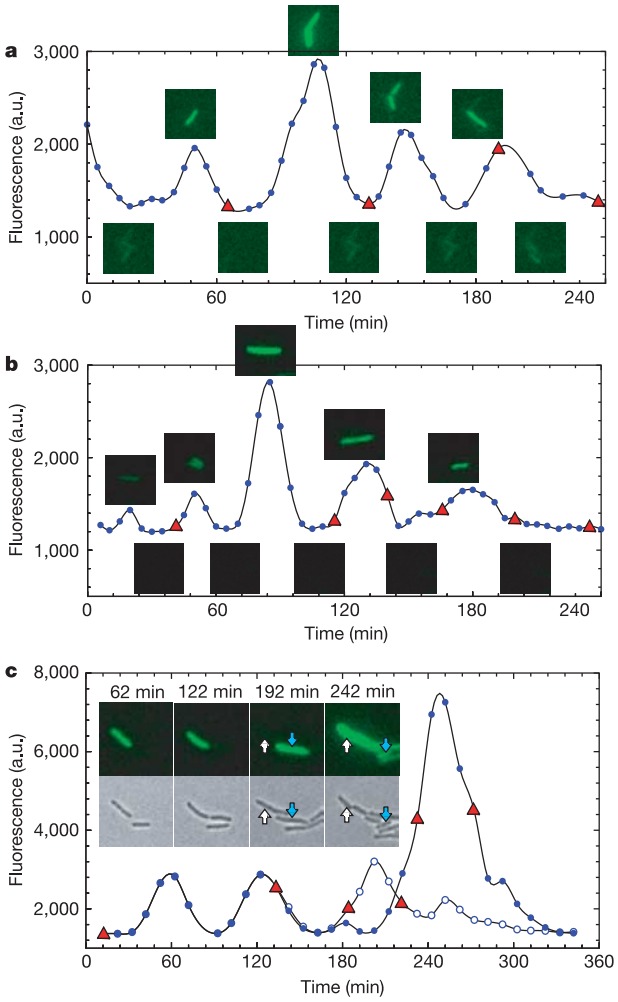

Figure 2 Oscillation dynamics of the metabolator in glucose. In each panel, red triangles denote cell division. Fluorescence intensity shown in arbitrary units. Inserts show the fluorescence intensities at peaks and valleys during oscillation. **a**, **b**, Representative single cell dynamics evaluated at 30 °C from ten independent experiments. **c**, Representative oscillation dynamics of two sibling cells evaluated at 37 °C from four independent experiments. The arrows (blue or white) in inserts point to sibling cells after cell division. Comparison of sibling cells shows skipped or delayed peaks (compare filled and open circles), which might be partially explained by uneven distribution of cellular materials.

M_1 level increases. E_1 is then expressed again and E_2 is degraded, returning the circuit to the first stage. On the other hand, if the input flux is low, M_2 does not accumulate sufficiently fast to cause a large swing in gene expression, and a stable steady state can be reached. This design allows metabolic physiology to influence gene expression cycles, a characteristic seen in circadian regulation.

Such a conceptual design was realized using the acetate pathway in *E. coli* (Fig. 1b). The M_1 pool is acetyl coenzyme A (acetyl-CoA) and the M_2 pool consists of acetyl phosphate (AcP), acetate (OAc^-) and the protonated form of acetate (HOAc). Acetyl-CoA is a metabolic product of sugar, fatty acids and some amino acids, and is the entry point into the tricarboxylic acid (TCA) cycle. Acetyl-CoA is converted to acetyl phosphate in *E. coli* by phosphate acetyltransferase (Pta), which corresponds to enzyme E_1 in Fig. 1a, and then to acetate by acetate kinase (Ack). The protonated form of acetate is permeable across the cell membrane. Under aerobic conditions, acetyl-CoA is further oxidized in the TCA cycle. The remaining flux goes to produce either acetate or ethanol. In wild-type *E. coli*, the enzyme acetyl-CoA synthetase (Acs) is induced in the presence of acetate[16]. However, such induction is under catabolite repression by glucose in the wild-type strain so as to avoid futile cycling. In our design, acetyl-CoA synthetase is used as enzyme E_2 in Fig. 1a. Thus, both phosphate acetyltransferase and acetyl-CoA synthetase need to be re-wired to respond to the M_2 pool.

Acetyl phosphate in the M_2 pool is used as a signalling molecule that activates the *glnAp2* promoter through phosphorylation of the nitrogen regulator I (NR_I or NtrC) in strains lacking the sensor, nitrogen regulator II (NR_{II} or NtrB), which is encoded by the *glnL* gene[5,11,17]. We used a Δ*glnL* strain as the host and placed the *acs* gene under the control of *glnAp2* promoter in a plasmid. When acetyl phosphate builds up, it activates the *glnAp2* promoter, which controls the expression of *acs*. At the same time, acetyl phosphate represses *pta* expression indirectly: a *glnAp2* promoter is used to control the production of the *lac* repressor (LacI), which in turn represses the expression of the *pta* gene from the *lacO-1* promoter[18]. The three proteins Acs, LacI and Pta are each fused with a degradation tag at their carboxy terminals so as to reduce their half-life[19].

We constructed the metabolator strain and plasmid according to the design shown in Fig. 1c. The host strain used was BW18793 (ref. 20), which contains *glnL* and *pta* null mutations and *lac* deletion. The *lacI* gene, controlled by the *glnAp2* promoter, was integrated into the chromosome using the CRIM method[21]. The *pta* and *acs* genes were cloned into plasmid pACYC184, under the control of *lacO1* and *glnAP2* promoters, respectively. To monitor the behaviour of the metabolator, a green fluorescent protein (GFP) fused with a degradation tag[19] was ligated downstream of a plasmid-borne LacI-repressible *tac* promoter, to be used as a readout. We demonstrated (see Supplementary Information) that the oscillation behaviour was insensitive to the degradation rate of GFP, which affects the phase but not the period of oscillation. Therefore, the period observed from the GFP readout reflects the dynamics of the system.

We monitored the GFP expression of individual cells grown on a thin agar gel with glucose and casamino acids under a fluorescence microscope at 30 °C (Fig. 2a, b) and 37 °C (Fig. 2c). About 60% of the initial colonies oscillate with varying amplitude and a period of 45 ± 10 min (mean ± s.d. for a total of 85 cells in 10 experiments), for a total duration of at least 4 h. The cell divisions (generation time ~60 min) appeared to be uncorrelated with the oscillation cycle, suggesting that the metabolator is responsible for the oscillation and is independent of the cell cycle. The baseline for the fluorescence and frequency of oscillation remained reasonably constant (Fig. 2a–c) but the amplitude varied. After division, the daughter cells commonly show uneven fluorescence (Fig. 2c), possibly because of stochastic variation in distributing cellular materials. Acetate was secreted from the cell, but was later shown to suppress rather than synchronize oscillation in both liquid and agar cultures.

To analyse the system quantitatively, we constructed a nonlinear ordinary differential equation (ODE) model on the basis of a dynamic balance of biomolecules. Enzyme kinetics were described by Michaelis–Menten kinetics and gene expression kinetics were

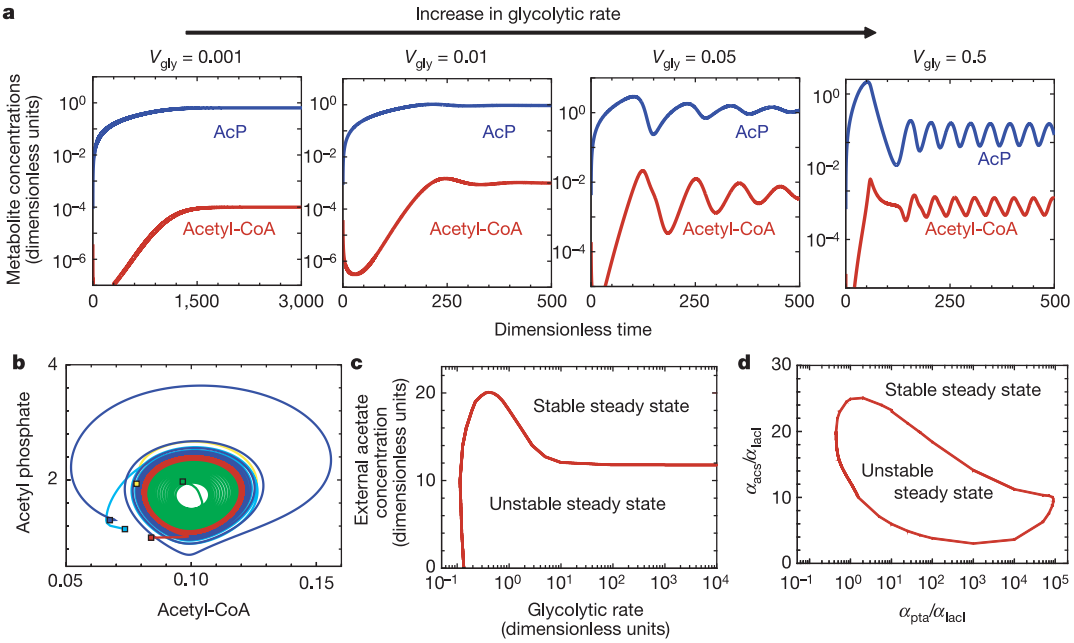

Figure 3 Computational characterization of the metabolator. **a**, The metabolator is prone to oscillate at increasing glycolytic rates (V_{gly}). V_{gly} in the four panels (from left to right) are 0.001, 0.01, 0.05 and 0.5. **b**, Phase plots constructed by perturbing steady state solution at $V_{gly} = 1$ reveal the oscillatory dynamics is limit cycle oscillation. Squares represent the initial state of the system. **c**, Phase diagram of glycolytic rate and external acetate concentration reveals the flux-sensitive oscillation behaviour of the metabolator. **d**, A phase diagram suggests that specific combinations of three proteins are necessary to support oscillation with $V_{gly} = 10$. α_i is related to the gene copy number for the synthesis of protein i (where i is LacI, Pta or Acs).

described using the Hill equation (see Supplementary Information). Numerical simulations show that with increased glycolytic flux, the system is prone to oscillate (Fig. 3a) and approach a limit cycle (Fig. 3b) regardless of the initial condition. Floquet analysis shows that the limit cycle is stable (see Supplementary Information). In addition, Hopf bifurcation analysis shows that the system operates at a stable, steady state at low glycolytic fluxes, but becomes oscillatory when the glycolytic flux increases above a critical point (Fig. 3c). On the other hand, increasing the external acetate concentration stabilizes the system and suppresses oscillation.

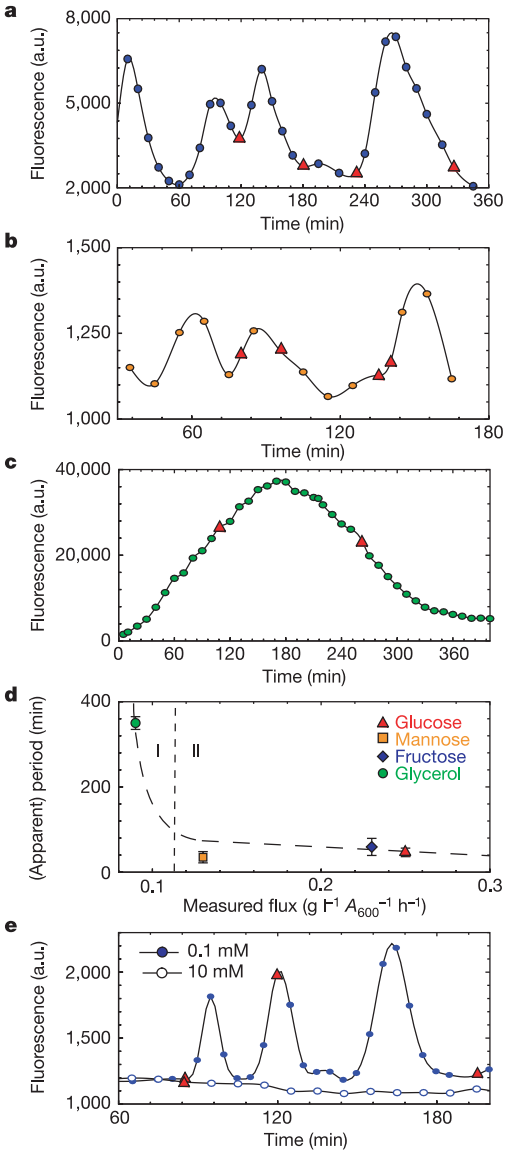

Figure 4 Flux-sensitive oscillation. Red triangles in **a**–**c** and **e** denote cell division. **a**–**c**, Dynamics using fructose (**a**), mannose (**b**) or glycerol (**c**) as a carbon source. **d**, Effect of glycolytic flux on period (fructose, glucose and mannose) and apparent period (glycerol). Apparent period is the time between the first and second valleys in a damped oscillation. The (apparent) periods are taken as the average of 85 (glucose), 32 (fructose), 18 (mannose) or 5 (glycerol) cells from three independent biological repeats. Glycolytic flux is evaluated by averaging at least three independent measurements. Error bars show standard deviation between repeats. Dashed line shows the theoretical correlation between (apparent) period and glycolytic flux. Region I denotes stable steady state and region II denotes a periodic state. **e**, Effect of acetate on metabolator dynamics. 10 mM external acetate suppressed oscillation but 0.1 mM did not.

To verify our theoretical predictions, we changed the glycolytic rate by varying the carbon source from glucose to less favourable carbon sources (fructose, mannose or glycerol) under otherwise identical conditions. Glycolytic flux decreased in the following order (from highest flux to lowest flux): glucose, fructose, mannose and glycerol (Fig. 4d). High glycolytic rates from glucose, fructose, and mannose supported oscillation (Figs 2 and 4a, b) but a low glycolytic rate from glycerol did not (Fig. 4c). Furthermore, addition of 10 mM acetate in the medium abolished oscillation (Fig. 4e), whereas 0.1 mM acetate still supported periodic behaviour. These data corroborate the results shown in Fig. 3c and demonstrate the role of glycolytic flux and acetate concentration on the dynamic behaviour of the metabolator.

We also used the model to explore the design parameter space of the metabolator. In particular, bifurcation analysis using the gene copy numbers of *acs* and *pta* relative to the chromosomal copy of *lacI* as parameters shows that the oscillation is characterized by an island defined by specific combinations of relative Acs and Pta levels (Fig. 3d). This analysis suggests that the relative gene copy number is an important determinant of oscillatory behaviour. This prediction is consistent with experimental results: when Acs was omitted in the metabolator, the system ceased to oscillate. Furthermore, the island of oscillation might partially explain the relatively few cycles of oscillation observed, as cell growth might move the system out of the oscillation region when the intracellular and extracellular environment changes. With biological stochasticity, some cells might operate outside of the oscillation island, and thus not all cells show oscillation.

The metabolator illustrates the use of metabolic fluxes to control biological oscillation. Specifically, oscillation is generated by the glycolytic flux leading to acetyl-CoA. Once the glycolytic flux exceeds a critical value, the system 'chokes' and begins to oscillate. However, this oscillation can be suppressed by imposing a sufficiently high concentration of acetate, which maintains an acetyl phosphate level outside of the dynamic range of the *glnAp2* promoter response. In the agar culture, accumulation of acetate produced from the cell eventually moves the system out of the oscillation region. Long-term observation of oscillation thus requires perfusion of the system.

The intrinsic noise in transcriptional regulation and the discrete nature of biological processes might explain some of the variations observed experimentally. For example, the amplitude of oscillation varied considerably. This variation was uncorrelated with cell division, and therefore, the intrinsic noise in gene expression processes appears to be responsible for determining oscillatory amplitude. Simulation results accounting for stochastic variations in the expression and degradation kinetics appear to explain the observed data (Supplementary Fig. S1). Upon cell division, sibling cells showed phase-shifts or peak omissions, possibly due to uneven distribution of cellular material that sets the daughter cells to a different phase of oscillation. In some cases, some daughter cells cease to oscillate, owing to a dramatic change in the relative levels of LacI, Acs and Pta.

The unique design of the metabolator represents a fusion of metabolic and transcriptional oscillation, and allows external carbon sources to influence oscillation. Natural metabolic oscillators, such as yeast glycolysis[1], are mainly based on allosteric enzyme regulation, which has a timescale of about 5 min. Purely transcriptional oscillators typically show a period of hours, with previous examples including 2.5 h (ref. 13) and 10 h (ref. 14). As a hybrid of metabolic and transcriptional oscillators, the metabolator shows an intermediate period (45 min); this is consistent with our expectations. The metabolator involves both negative feedback (E_1) and positive feed-forward (E_2) regulation. Negative feedback is typically used to stabilize a system, however, it tends to be unstable if the time lag in feedback increases. Negative feedback systems in a loop design can also generate oscillation[13].

The function of metabolator is somewhat analogous to the circadian clock, in that both are integrated with metabolic physiology and respond to external stimuli (carbon sources in the former, light in the latter). The close involvement of metabolism in circadian regulation has been documented. For example, metabolic entrainment[22,23] is recognized as serving important physiological roles. Haem biosynthesis is known to be regulated by the circadian clock[24] and acetyl-CoA has been shown to participate in the conversion of serotonin to *N*-acetylserotonin, which is responsible for the melatonin circadian rhythm in vertebrates[25]. The metabolator might provide useful insights into the operating principles of physiologically integrated natural oscillators. Moreover, the role of metabolic flux in controlling oscillation demonstrated here suggests that network connectivity alone is insufficient to determine cellular behaviour. In addition to mapping the regulatory wiring diagram in cells, dynamic characterization will also be essential. □

Methods

Bacterial strains and plasmids

The *lacI* gene under the control of the *glnAp2* promoter was inserted into the chromosome of *E. coli* BW18793 (ref. 20) at the lambda attachment site (att_λ) using the CRIM method[21] to produce the host strain. The *glnAp2*, *tac* and *lacO-1* promoters were obtained from p2IDI (ref. 5), pKK223-3 (ref. 26) and pZE12 (ref. 18), respectively. The *pta* gene was cloned by polymerase chain reaction from the *Bacillus subtilis* chromosome. The *acs* and *lacI* genes were cloned from the *E. coli* MG1655 chromosome. For both *pta* and *lacI*, the GTG start codon was changed to ATG using their respective 5′ primers. The 11-amino-acid *ssrA* tag[27] was added to the genes of the metabolator via the 3′ primers. The resulting protein, carrying the peptide tag, is recognized and targeted for degradation by tail-specific Tsp proteases. The pEF3 plasmid was constructed in two sequential cloning steps from intermediate plasmids containing the two genes into pACYC184. The reporter plasmid was constructed by cloning *gfpmut3.1* with the degradation tag into pKK223-3.

Microscopy and analysis of gene expression

Cells were grown at 37 °C in M9 media with 0.4% of an appropriate carbon source (glucose, fructose, mannose or glycerol), 0.1% casamino acids and antibiotics (5 μg ml^{-1} kanamycin, 25 μg ml^{-1} chloramphenicol and 100 μg ml^{-1} ampicillin) and harvested when the absorbance at 600 nm reached 0.5–1.3. Cells were concentrated by centrifugation and the resulting pellet was resuspended in 1 ml growth medium for preparation of microscope slides. Time-lapse microscopy was performed using a Nikon TE2000-S microscope with a × 60 DIC oil immersion objective. Images were captured using a 512 × 512–pixel cooled CCD camera controlled through Metamorph software. An agar pad was created as described in ref. 28. The temperature of the samples was maintained at approximately 30 °C by an objective heater. Brightfield (0.1 s) and epifluorescence (0.1 s) images were captured every 5 min, with both light sources shuttered between exposures. All image analysis was done using Metamorph. Cells from the final frame of the brightfield video image were randomly chosen and manually tracked back to the first frame. In each frame of the brightfield image, regions were drawn around cells using Metamorph and transferred to the fluorescence image, and the average intensities of the regions were recorded.

Each of the fluorescence measurements for the metabolator dynamics was obtained from at least three independent cultures. For each culture, at least 60% of the cells were tracked for GFP dynamics in response to oscillation induced by glucose ($n = 85$, Fig. 2), fructose ($n = 32$, Fig. 4a), mannose ($n = 18$, Fig. 4b), glycerol ($n = 5$, Fig. 4c) or two different concentrations of acetate ($n = 27$, Fig. 4e). In addition, various negative controls were conducted. These included fluorescence measurements for the metabolator supplemented with 100 μM isopropyl-β-D-thiogalactoside (IPTG), for the host strain containing a reporter plasmid only, and for the host strain with a chromosome-integrated *pta* gene under the control of the *tac* promoter and the reporter plasmid.

Glycolytic flux measurements

The oscillation strain (without the reporter plasmid) was grown overnight in M9 media containing 0.4% of an appropriate carbon source, as described above. Cells were then collected by centrifugation and resuspended to an absorbance at 600 nm of 0.5 in fresh M9 media containing 0.1% casamino acids, antibiotics and 0.04% carbon source. Samples were collected every 30 min for supernatant and cell density measurements. Cell density was measured in triplicate using a microplate reader. Glucose and fructose concentrations were measured in triplicate with a D-glucose/D-fructose kit and glycerol was measured with a glycerol kit (R-biopharm), in accordance with the manufacturer's instructions. Mannose was measured using a dinitrosalicylic acid (DNS) assay. Carbon flux was calculated on the basis of sugar consumption.

Physicochemical modelling and numerical analysis

A nonlinear ODE-based model was developed to describe the key components of the metabolator. Exact expressions of the model are presented in the Supplementary Information. The computational approach used to elucidate the dynamics and behaviour of this model involves two components. First, direct numerical simulation was conducted to explore the nonlinear dynamics of the model (for example, Fig. 3a). The exact parameter values used in this simulation are shown in Supplementary Table S1. Next, phase diagrams that mapped out the location of Hopf bifurcation as functions of key parameters were constructed to study the asymptotic behaviour of the model[29]. Each phase diagram was constructed by mapping the locus of Hopf bifurcation as a function of key parameters. Specifically, the response of the steady-state solution to infinitesimal perturbations was computed by solving a linearized model about the same steady state. This linear response is determined by calculation of the eigenvalues in the linear spectrum that have the largest real part, σ. The onset of the Hopf bifurcation is determined by the moment at which the real part of a complex conjugate pair of eigenvalues of the jacobian matrix crosses zero, while the real parts of all other eigenvalues remain negative.

Received 16 November 2004; accepted 28 February 2005; doi:10.1038/nature03508.

1. Goldbeter, A. *Biochemical Oscillations and Cellular Rhythms: The Molecular Bases of Periodic and Chaotic Behaviour* (Cambridge Univ. Press, New York, 1996).
2. Hess, B. Periodic patterns in biology. *Naturwissenschaften* **87,** 199–211 (2000).
3. Bier, M., Teusink, B., Kholodenko, B. N. & Westerhoff, H. V. Control analysis of glycolytic oscillations. *Biophys. Chem.* **62,** 15–24 (1996).
4. Bier, M., Bakker, B. M. & Westerhoff, H. V. How yeast cells synchronize their glycolytic oscillations: a perturbation analytical treatment. *Biophys. J.* **78,** 1087–1093 (2000).
5. Farmer, W. R. & Liao, J. C. Improving lycopene production in *Escherichia coli* by engineering metabolic control. *Nature Biotechnol.* **18,** 533–537 (2000).
6. Gardner, T. S., Cantor, C. R. & Collins, J. J. Construction of a genetic toggle switch in *Escherichia coli*. *Nature* **403,** 339–342 (2000).
7. Becskei, A., Seraphin, B. & Serrano, L. Positive feedback in eukaryotic gene networks: cell differentiation by graded to binary response conversion. *EMBO J.* **20,** 2528–2535 (2001).
8. Guet, C. C., Elowitz, M. B., Hsing, W. & Leibler, S. Combinatorial synthesis of genetic networks. *Science* **296,** 1466–1470 (2002).
9. Isaacs, F. J., Hasty, J., Cantor, C. R. & Collins, J. J. Prediction and measurement of an autoregulatory genetic module. *Proc. Natl Acad. Sci. USA* **100,** 7714–7719 (2003).
10. Basu, S., Mehreja, R., Thiberge, S., Chen, M. T. & Weiss, R. Spatiotemporal control of gene expression with pulse-generating networks. *Proc. Natl Acad. Sci. USA* **101,** 6355–6360 (2004).
11. Bulter, T. *et al.* Design of artificial cell–cell communication using gene and metabolic networks. *Proc. Natl Acad. Sci. USA* **101,** 2299–2304 (2004).
12. You, L., Cox, R. S. III, Weiss, R. & Arnold, F. H. Programmed population control by cell–cell communication and regulated killing. *Nature* **428,** 868–871 (2004).
13. Elowitz, M. B. & Leibler, S. A synthetic oscillatory network of transcriptional regulators. *Nature* **403,** 335–338 (2000).
14. Atkinson, M. R., Savageau, M. A., Myers, J. T. & Ninfa, A. J. Development of genetic circuitry exhibiting toggle switch or oscillatory behavior in *Escherichia coli*. *Cell* **113,** 597–607 (2003).
15. Kobayashi, H. *et al.* Programmable cells: interfacing natural and engineered gene networks. *Proc. Natl Acad. Sci. USA* **101,** 8414–8419 (2004).
16. Kumari, S. *et al.* Regulation of acetyl coenzyme A synthetase in *Escherichia coli*. *J. Bacteriol.* **182,** 4173–4179 (2000).
17. McCleary, W. R. & Stock, J. B. Acetyl phosphate and the activation of two-component response regulators. *J. Biol. Chem.* **269,** 31567–31572 (1994).
18. Lutz, R. & Bujard, H. Independent and tight regulation of transcriptional units in *Escherichia coli* via the LacR/O, the TetR/O and AraC/I1–I2 regulatory elements. *Nucleic Acids Res.* **25,** 1203–1210 (1997).
19. Andersen, J. B. *et al.* New unstable variants of green fluorescent protein for studies of transient gene expression in bacteria. *Appl. Environ. Microbiol.* **64,** 2240–2246 (1998).
20. Feng, J. *et al.* Role of phosphorylated metabolic intermediates in the regulation of glutamine synthetase synthesis in *Escherichia coli*. *J. Bacteriol.* **174,** 6061–6070 (1992).
21. Haldimann, A. & Wanner, B. L. Conditional-replication, integration, excision, and retrieval plasmid-host systems for gene structure-function studies of bacteria. *J. Bacteriol.* **183,** 6384–6393 (2001).
22. Rutter, J., Reick, M. & McKnight, S. L. Metabolism and the control of circadian rhythms. *Annu. Rev. Biochem.* **71,** 307–331 (2002).
23. Rutter, J., Reick, M., Wu, L. C. & McKnight, S. L. Regulation of clock and NPAS2 DNA binding by the redox state of NAD cofactors. *Science* **293,** 510–514 (2001).
24. Kaasik, K. & Lee, C. C. Reciprocal regulation of haem biosynthesis and the circadian clock in mammals. *Nature* **430,** 467–471 (2004).
25. Ferry, G. *et al.* Substrate specificity and inhibition studies of human serotonin N-acetyltransferase. *J. Biol. Chem.* **275,** 8794–8805 (2000).
26. Brosius, J. & Holy, A. Regulation of ribosomal RNA promoters with a synthetic lac operator. *Proc. Natl Acad. Sci. USA* **81,** 6929–6933 (1984).
27. Keiler, K. C., Waller, P. R. & Sauer, R. T. Role of a peptide tagging system in degradation of proteins synthesized from damaged messenger RNA. *Science* **271,** 990–993 (1996).
28. Rines, D. R., He, X. & Sorger, P. K. Quantitative microscopy of green fluorescent protein-labeled yeast. *Methods Enzymol.* **351,** 16–34 (2002).
29. Iooss, G. & Joseph, D. D. *Elementary Stability and Bifurcation Theory* (Springer-Verlag, New York, 1989).

Supplementary Information accompanies the paper on **www.nature.com/nature**.

Acknowledgements The authors thank V. Roychowdhury and J. Bridgewater for discussions. This work was partially funded by the Center for Cell Mimetic Space Exploration, a National Aeronautics and Space Administration University Research, Engineering, and Technology Institute. J.C.L. is a member of California NanoSystems Institute and UCLA-DOE Institute for Genomics and Proteomics.

Competing interests statement The authors declare that they have no competing financial interests.

Correspondence and requests for materials should be addressed to J.C.L. (liaoj@ucla.edu).